Article

Growth and Assembly of Crystalline Tungsten Oxide Nanostructures Assisted by Bioligation

Julien Polleux, Nicola Pinna, Markus Antonietti, and Markus Niederberger

J. Am. Chem. Soc., **2005**, 127 (44), 15595-15601• DOI: 10.1021/ja0544915 • Publication Date (Web): 18 October 2005

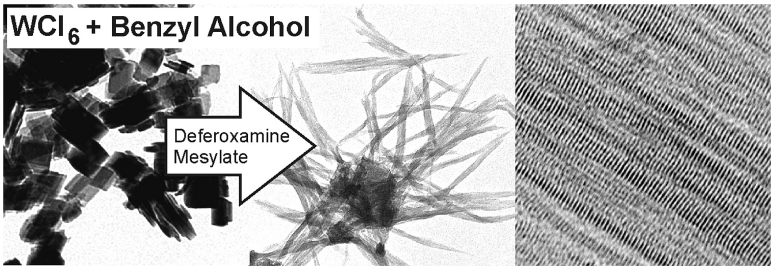

More About This Article

Additional resources and features associated with this article are available within the HTML version:

- Supporting Information
- Links to the 16 articles that cite this article, as of the time of this article download
- Access to high resolution figures
- Links to articles and content related to this article
- Copyright permission to reproduce figures and/or text from this article

View the Full Text HTML

J|A|C|S
ARTICLES
Published on Web 10/18/2005

Growth and Assembly of Crystalline Tungsten Oxide Nanostructures Assisted by Bioligation

Julien Polleux,[†] Nicola Pinna,[‡] Markus Antonietti,[†] and Markus Niederberger*[,†]

Contribution from the Max-Planck-Institute of Colloids and Interfaces, Colloid Chemistry, Research Campus Golm, 14424 Potsdam, Germany, and Martin-Luther-Universität Halle-Wittenberg, Institut für Anorganische Chemie, Kurt-Mothes-Strasse 2, 06120 Halle (Saale), Germany

Received July 7, 2005; E-mail: markus.niederberger@mpikg.mpg.de

Abstract: Here, we present a systematic study on the influence of the bioligand deferoxamine mesylate on the crystallization and assembly behavior of tungsten oxide in a soft-chemistry process. Without deferoxamine mesylate, this approach yields pseudo-single crystalline tungstite nanoplatelets consisting of a large number of crystallographically almost perfectly aligned primary crystallites. In the presence of a constant amount of deferoxamine, the particle morphology drastically changes with temperature, ranging from wormlike organic−inorganic hybrid nanostructures to single-crystalline tungsten oxide nanowires, highlighting the role of the bioligand in controlling the crystal growth and assembly behavior. The nanowires have a uniform diameter of about 1.3 nm, an aspect ratio of more than 500, and the structural flexibility of tungsten oxide. The presented process is based on the combination of biomimetic construction principles with nonaqueous sol−gel chemistry, thus combining the advantages of both tools, excellent control over particle morphology and high crystallinity at low temperature.

Introduction

The controlled synthesis and characterization of one-dimensional nanostructures is a fascinating objective in modern materials science, chemistry, and physics. The high interest lies in the fact that nanowires and nanotubes represent the smallest objects for efficient transport of electrons and excitons, and thus are particularly attractive building blocks for hierarchical assembly of functional nanoscale structures.[1−3] In view of the importance of these materials, diverse synthesis methodologies involving vapor phase techniques and solution-growth processes have been used, covering a wide variety of compositions ranging from elements, oxides, nitrides, and carbides to chalcogenides.[4,5] In this context, it is interesting to note that, although transition metal oxides constitute one of the most important classes of materials, their synthesis in the form of crystalline objects with one-dimensional morphology is still restricted to a few examples.[6] The most prominent ones include vanadium,[7−9] titanium,[10,11] molybdenum,[12] tungsten,[13] and iron oxide nanotubes,[14] as well as titanium,[15] manganese,[16] molybdenum,[17−19] copper,[20,21] and vanadium oxide nanowires.[22−27]

In addition to the spontaneous self-assembly of preformed nanocrystals into nanowires,[28−32] especially biomimetic syn-

[†] Max-Planck-Institute of Colloids and Interfaces.
[‡] Martin-Luther-Universität Halle-Wittenberg.

(1) Tans, S. J.; Verschueren, A. R. M.; Dekker, C. *Nature* **1998**, *393*, 49.
(2) Duan, X. F.; Huang, Y.; Cui, Y.; Wang, J. F.; Lieber, C. M. *Nature* **2001**, *409*, 66.
(3) Huang, Y.; Duan, X. F.; Wei, Q. Q.; Lieber, C. M. *Science* **2001**, *291*, 630.
(4) Rao, C. N. R.; Deepak, F. L.; Gundiah, G.; Govindaraj, A. *Prog. Solid State Chem.* **2003**, *31*, 5.
(5) Xia, Y. N.; Yang, P. D.; Sun, Y. G.; Wu, Y. Y.; Mayers, B.; Gates, B.; Yin, Y. D.; Kim, F.; Yan, Y. Q. *Adv. Mater.* **2003**, *15*, 353.
(6) Patzke, G. R.; Krumeich, F.; Nesper, R. *Angew. Chem., Int. Ed.* **2002**, *41*, 2446.
(7) Spahr, M. E.; Bitterli, P.; Nesper, R.; Muller, M.; Krumeich, F.; Nissen, H. U. *Angew. Chem., Int. Ed.* **1998**, *37*, 1263.
(8) Krumeich, F.; Muhr, H. J.; Niederberger, M.; Bieri, F.; Schnyder, B.; Nesper, R. *J. Am. Chem. Soc.* **1999**, *121*, 8324.
(9) Niederberger, M.; Muhr, H. J.; Krumeich, F.; Bieri, F.; Günther, D.; Nesper, R. *Chem. Mater.* **2000**, *12*, 1995.
(10) Kasuga, T.; Hiramatsu, M.; Hoson, A.; Sekino, T.; Niihara, K. *Langmuir* **1998**, *14*, 3160.
(11) Saponjic, Z. V.; Dimitrijevic, N. M.; Tiede, D. M.; Goshe, A. J.; Zuo, X.; Chen, L. X.; Barnard, A. S.; Zapol, P.; Curtiss, L.; Rajh, T. *Adv. Mater.* **2005**, *17*, 965.
(12) Li, Y.; Bando, Y. *Chem. Phys. Lett.* **2002**, *364*, 484.
(13) Li, Y. B.; Bando, Y.; Golberg, D. *Adv. Mater* **2003**, *15*, 1294.
(14) Liu, Z.; Zhang, D.; Han, S.; Li, C.; Lei, B.; Lu, W.; Fang, J.; Zhou, C. *J. Am. Chem. Soc.* **2005**, *127*, 6.
(15) Jiang, X.; Wang, Y.; Herricks, T.; Xia, Y. *J. Mater. Chem.* **2004**, *14*, 695.
(16) Wang, X.; Li, Y. *J. Am. Chem. Soc.* **2002**, *124*, 2880.
(17) Niederberger, M.; Krumeich, F.; Muhr, H. J.; Müller, M.; Nesper, R. *J. Mater. Chem.* **2001**, *11*, 1941.
(18) Lou, X. W.; Zeng, H. C. *J. Am. Chem. Soc.* **2003**, *125*, 2697.
(19) Patzke, G. R.; Michailovski, A.; Krumeich, F.; Nesper, R.; Grunwaldt, J. D.; Baiker, A. *Chem. Mater.* **2004**, *16*, 1126.
(20) Jiang, X.; Herricks, T.; Xia, Y. *Nano Lett.* **2002**, *2*, 1333.
(21) Xiong, Y.; Li, Z.; Zhang, R.; Xie, Y.; Yang, J.; Wu, C. *J. Phys. Chem. B* **2003**, *107*, 3697.
(22) Muster, J.; Kim, G. T.; Krstic, V.; Park, J. G.; Park, Y. W.; Roth, S.; Burghard, M. *Adv. Mater.* **2000**, *12*, 420.
(23) Pinna, N.; Wild, U.; Urban, J.; Schlögl, R. *Adv. Mater.* **2003**, *15*, 329.
(24) Pinna, N.; Willinger, M.; Weiss, K.; Urban, J.; Schlögl, R. *Nano Lett.* **2003**, *3*, 1131.
(25) Gu, G.; Schmid, M.; Chiu, P. W.; Minett, A.; Fraysse, J.; Kim, G. T.; Roth, S.; Kozlov, M.; Munoz, E.; Baughman, R. H. *Nat. Mater.* **2003**, *2*, 316.
(26) Guiton, B. S.; Gu, Q.; Prieto, A. L.; Gudiksen, M. S.; Park, H. *J. Am. Chem. Soc.* **2005**, *127*, 498.
(27) Liu, J.; Wang, X.; Peng, Q.; Li, Y. *Adv. Mater.* **2005**, *17*, 764.
(28) Tang, Z. Y.; Kotov, N. A.; Giersig, M. *Science* **2002**, *297*, 237.
(29) Pacholski, C.; Kornowski, A.; Weller, H. *Angew. Chem., Int. Ed.* **2002**, *41*, 1188.
(30) Polleux, J.; Pinna, N.; Antonietti, M.; Niederberger, M. *Adv. Mater.* **2004**, *16*, 436.

thesis approaches are promising for the soft-chemistry fabrication of anisotropic materials.[33−35] In aqueous systems, hydrophilic polymer controlled morphosynthesis has proven to be a versatile approach for the preparation of inorganic materials with unusual morphological complexity.[36] This approach is in strong contrast to the surfactant-mediated templating techniques that have been widely exploited in controlling the shape and size of semiconductors.[37] Hydrophilic polymers do not act as supramolecular templates, but play the role of soluble species being active at various hierarchy levels of the forming mineral hybrid.[38] Up to now, morphosynthesis of crystalline transition metal oxides has scarcely been reported, mainly due to the fact that metal oxide precursors such as metal halides and metal alkoxides exhibit fast hydrolysis and condensation rates. Therefore, the morphosynthesis of transition metal oxides has to overcome the problem that sol−gel-derived materials at low temperature are amorphous and that the necessary heat treatment to induce crystallization is usually accompanied by undesired alteration of particle morphology. Nonaqueous sol−gel processes offer an elegant solution to this problem, as they result in the formation of crystalline metal oxide nanoparticles at low temperatures.[39−44]

To bring together nonaqueous sol−gel chemistry and morphosynthesis, we performed a detailed study on the influence of the siderophore deferoxamine mesylate (DFOM) on the crystallization and assembly behavior of tungsten oxide in comparison to a reference experiment without deferoxamine. Among the transition metal oxides, tungsten oxide is of particular scientific and technological interest, because its optical and electronic properties make it a promising candidate for applications in electrochromic[45−49] and sensing[50−53] devices. Our synthesis approach involves a simple one-pot reaction of tungsten chloride with benzyl alcohol with and without DFOM at various reaction temperatures in a glass vial. Deferoxamine contains three hydroxamic acid groups (RCONR′OH), one of the most powerful bioligating moieties[54] with a rich coordination chemistry,[55] and two amide groups, potentially providing intermolecular amide−amide interactions similar to proteins, and thus offering the possibility of supramolecular assembly. Deferoxamine belongs to the family of siderophores, a class of low-molecular weight iron-coordinating agents produced by microbial organisms, and is therefore commercially available on larger scales. It is also used clinically in the treatment of iron overload disease.[56] Binary mixtures of benzyl alcohol and amides feature various molecular interactions[57] and possibly also promote amide−amide interactions between two deferoxamine molecules. Furthermore, benzyl alcohol has already proven to be a particularly versatile solvent for the soft-chemistry synthesis of transition metal oxide nanocrystals[58−63] and lamellar nanohybrids.[64]

Experimental Details

In a typical synthesis, 200 mg of tungsten chloride WCl_6 (99.9%; Aldrich) was dissolved in 13 mL of anhydrous benzyl alcohol (99.8%; Aldrich) in a glass beaker. After being stirred for a few minutes, the solution turned blue and 36.8 mg of deferoxamine mesylate (95%; Aldrich) was added. The molar ratio of tungsten to deferoxamine is 9. The vial was sealed, and the mixture was heated under stirring at various temperatures for 48 h in a preheated oil bath. The product was collected by centrifugation, thoroughly washed with ethanol, and dried at 60 °C. The yield is about 60%.

The X-ray powder diffraction (XRD) diagrams of all samples were measured in reflection mode (Cu Kα radiation) on a Bruker D8 diffractometer equipped with a scintillation counter. The SAXS measurement was carried using a Nonius rotating anode ($P = 4$ kW, Cu Kα) with pinhole-collimation and a MARCCD detector for data acquisition. The sample−detector distance was 74.5 cm. 2D diffraction patterns obtained from the rotating anode setup were transformed into a 1D radial average of the scattering intensity. Transmission electron microscopy (TEM) investigations were performed either on an Omega 912 (Carl Zeiss) microscope, operated at 100 kV, or on a Philips CM200 FEG microscope, operated at 200 kV (HRTEM). Elemental analyses were carried out on a Vario EL Elementar (Elementar Analysensysteme, Hanau, Germany). Thermogravimetric analyses (TGA) were performed on a Netzsch TG 209, and IR investigations were performed on a Perkin-Elmer 2000 FTIR spectrometer.

Results and Discussion

The system tungsten chloride−benzyl alcohol provides a powerful means to tailor the morphology of tungsten oxide nanostructures in dependence of reaction parameters such as temperature and addition of a bioligand. To highlight the

(31) Polleux, J.; Pinna, N.; Antonietti, M.; Hess, C.; Wild, U.; Schlögl, R.; Niederberger, M. *Chem.-Eur. J.* **2005**, *11*, 3541.
(32) Tang, Z.; Kotov, N. A. *Adv. Mater.* **2005**, *17*, 951.
(33) Cha, J. N.; Stucky, G. D.; Morse, D. E.; Deming, T. J. *Nature* **2000**, *403*, 289.
(34) Mao, C. B.; Solis, D. J.; Reiss, B. D.; Kottmann, S. T.; Sweeney, R. Y.; Hayhurst, A.; Georgiou, G.; Iverson, B.; Belcher, A. M. *Science* **2004**, *303*, 213.
(35) Chan, C. S.; Stasio, G. D.; Welch, S. A.; Girasole, M.; Frazer, B. H.; Nesterova, M. V.; Fakra, S.; Banfield, J. F. *Science* **2004**, *303*, 1656.
(36) Yu, S. H.; Cölfen, H. *J. Mater. Chem.* **2004**, *14*, 2124.
(37) Peng, X. G.; Manna, L.; Yang, W. D.; Wickham, J.; Scher, E.; Kadavanich, A.; Alivisatos, A. P. *Nature* **2000**, *404*, 59.
(38) Cölfen, H.; Mann, S. *Angew. Chem., Int. Ed.* **2003**, *42*, 2350.
(39) Cozzoli, P. D.; Kornowski, A.; Weller, H. *J. Am. Chem. Soc.* **2003**, *125*, 14539.
(40) Niederberger, M.; Bartl, M. H.; Stucky, G. D. *J. Am. Chem. Soc.* **2002**, *124*, 13642.
(41) Niederberger, M.; Bartl, M. H.; Stucky, G. D. *Chem. Mater.* **2002**, *14*, 4364.
(42) Niederberger, M.; Garnweitner, G.; Krumeich, F.; Nesper, R.; Cölfen, H.; Antonietti, M. *Chem. Mater.* **2004**, *16*, 1202.
(43) Tang, J.; Redl, F.; Zhu, Y.; Siegrist, T.; Brus, L. E.; Steigerwald, M. L. *Nano Lett.* **2005**, *5*, 543.
(44) Ba, J.; Polleux, J.; Antonietti, M.; Niederberger, M. *Adv. Mater.* **2005**, *17*, 2509.
(45) Granqvist, C. G. *Sol. Energy Mater. Sol. Cells* **2000**, *60*, 201.
(46) Livage, J.; Ganguli, D. *Sol. Energy Mater. Sol. Cells* **2001**, *68*, 365.
(47) Santato, C.; Odziemkowski, M.; Ulmann, M.; Augustynski, J. *J. Am. Chem. Soc.* **2001**, *123*, 10639.
(48) Cheng, W.; Baudrin, E.; Dunn, B.; Zink, J. I. *J. Mater. Chem.* **2001**, *11*, 92.
(49) Azens, A.; Avendaño, E.; Backholm, J.; Berggren, L.; Gustavsson, G.; Karmhag, R.; Niklasson, G. A.; Roos, A.; Granqvist, C. G. *Mater. Sci. Eng., B* **2005**, *119*, 214.
(50) Prasad, A. K.; Gouma, P. I. *J. Mater. Sci.* **2003**, *38*, 4347.
(51) Berger, O.; Hoffmann, T.; Fischer, W.-J.; Melev, V. *J. Mater. Sci.: Mater. Electron.* **2004**, *15*, 483−493.
(52) Eranna, G.; Joshi, B. C.; Runthala, D. P.; Gupta, R. P. *Crit. Rev. Solid State Mater. Sci.* **2004**, *29*, 111.
(53) György, E.; Socol, G.; Mihailescu, I. N.; Ducu, C.; Ciuca, S. *J. Appl. Phys.* **2005**, *97*, 093527.
(54) Marmion, C. J.; Griffith, D.; Nolan, K. B. *Eur. J. Inorg. Chem.* **2004**, 3003.
(55) Kurzak, B.; Kozowski, H.; Farkas, E. *Coord. Chem. Rev.* **1992**, *114*, 169.
(56) Chaston, T. B.; Richardson, D. R. *Am. J. Hematol.* **2003**, *73*, 200.
(57) Ali, A.; Nain, A. K. *Bull. Chem. Soc. Jpn.* **2002**, *75*, 681.
(58) Niederberger, M.; Pinna, N.; Polleux, J.; Antonietti, M. *Angew. Chem., Int. Ed.* **2004**, *43*, 2270.
(59) Niederberger, M.; Garnweitner, G.; Pinna, N.; Antonietti, M. *J. Am. Chem. Soc.* **2004**, *126*, 9120.
(60) Pinna, N.; Neri, G.; Antonietti, M.; Niederberger, M. *Angew. Chem., Int. Ed.* **2004**, *43*, 4345−4349.
(61) Pinna, N.; Garnweitner, G.; Antonietti, M.; Niederberger, M. *Adv. Mater.* **2004**, *16*, 2196.
(62) Pinna, N.; Antonietti, M.; Niederberger, M. *Colloids Surf., A* **2004**, *250*, 211.
(63) Pinna, N.; Grancharov, S.; Beato, P.; Bonville, P.; Antonietti, M.; Niederberger, M. *Chem. Mater.* **2005**, *17*, 3044.
(64) Pinna, N.; Garnweitner, G.; Beato, P.; Niederberger, M.; Antonietti, M. *Small* **2005**, *1*, 113.

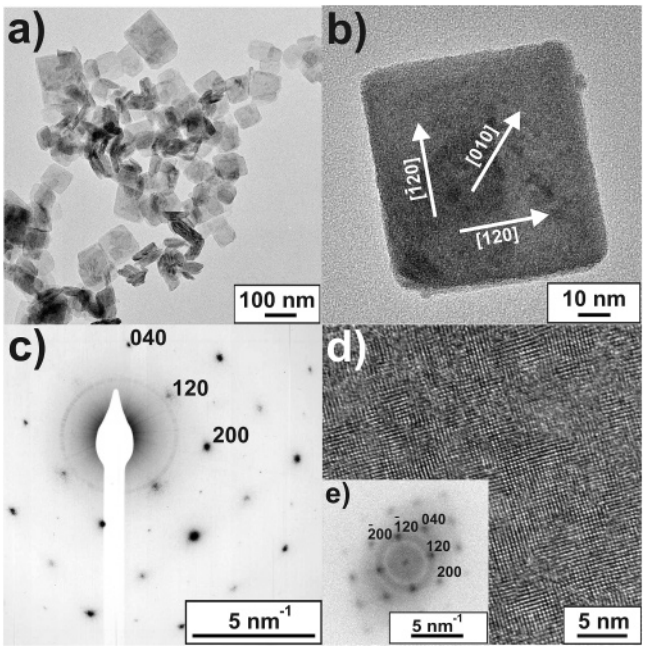

Figure 1. (a) TEM overview image of the tungstite nanoplatelets, (b) TEM image and (c) selected area electron diffraction (SAED) of one platelet oriented along the [001] direction, (d) HRTEM of a part of the platelet, and (e) its power spectrum (PS).

influence of DFOM on the crystallization and assembly behavior of tungsten oxide, this report is divided into two parts. First, we discuss the reference experiment, where tungsten oxide nanoplatelets are formed just by reacting tungsten chloride with benzyl alcohol without DFOM. In the second part, we present the effect of a constant concentration of DFOM at various temperatures on the particle morphology of tungsten oxide.

Figure 1 displays transmission electron microscopy (TEM) investigations of the tungsten oxide nanoparticles obtained in the reference experiment without the use of any ligand at 100 °C. An overview image is given in Figure 1a and shows that the particles exhibit a platelet-like shape with sides ranging from 30 to 100 nm. Side views on particles that are oriented vertically to the TEM copper grid reveal that they are sometimes stacked together and that their thickness is between 5 and 10 nm. The TEM image of an isolated platelet shows a square and well faceted shape (Figure 1b). The selected area electron diffraction pattern (SAED) recorded from this particle is composed of dark spots giving evidence that the particle behaves similar to a single crystal (Figure 1c). The measured lattice distances correspond to the orthorhombic tungstite $WO_3 \cdot H_2O$ structure (JCPDS 43-679). Surprisingly, a high-resolution TEM image of a part of a platelet demonstrates that the platelets exhibit an internal composite structure, which means that the particle is formed by fusion of a large number of small crystallites, just a few nanometers in size (Figure 1d). The inner structure becomes visible as there is some misalignment of the orientation of these particles with respect to each other, leading to defects, which are additionally indicated by diffuse reflection spots in the power spectrum (PS) (Figure 1e) of this HRTEM image. Analogous mesocrystals consisting of smaller crystallites, nevertheless behaving like single crystals, have recently been reported for iron oxide platelets,[65] calcium carbonate,[66] and others.[67]

(65) Niederberger, M.; Krumeich, F.; Hegetschweiler, K.; Nesper, R. *Chem. Mater.* **2002**, *14*, 78.

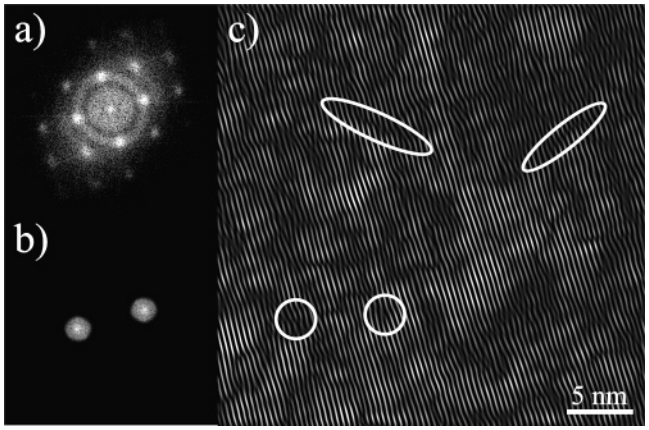

Figure 2. Fourier analysis of the HRTEM image in Figure 1d. (a) PS of Figure 1d, (b) masked PS, and (c) back Fourier transform of Figure 2b.

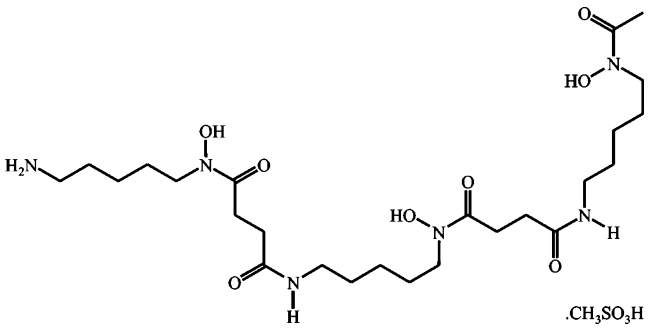

Figure 3. Chemical structure of deferoxamine mesylate.

One possibility for investigating the defects of a thin material in more detail is the Fourier analysis, which involves the masking of the calculated PS of a HRTEM image to get information from one pair of spots, followed by another back Fourier transform, so that a calculated HRTEM image is regenerated. With this approach, only the lattice planes corresponding to the reflections masked in the PS are obtained.

An example of such a Fourier analysis is given in Figure 2. In this case, application of a mask (Figure 2b) to the PS (Figure 2a) of the HRTEM image (Figure 1d) provides information about the 120 lattice planes. Figure 2c corresponds to the back Fourier transform of Figure 2b and shows that the lattice planes of the superstructure are all oriented in the same direction, however, also indicating the small misalignments. In addition, single dislocations (marked by the two circles in Figure 2c) as well as larger zones of misalignments of several planes (highlighted by the two ellipsoids) can be identified. These types of crystal defects suggest that platelet formation presumably occurs by oriented attachment[68,69] of primary crystallites leading to a two-dimensional arrangement of nanoparticles.

In a next step, the influence of DFOM on the crystallization of tungsten oxide is investigated. Figure 3 displays the chemical structure of DFOM. The addition of DFOM during the nanoparticle synthesis leads to totally different morphologies with respect to the reference experiment. Figure 4 gives a comparison of representative transmission electron micrographs of nanostructures obtained with a constant tungsten chloride-to-DFOM molar ratio of 9 in dependence of the synthesis temperature.

(66) Wang, T.; Cölfen, H.; Antonietti, M. *J. Am. Chem. Soc.* **2005**, *127*, 3246.
(67) Cölfen, H.; Antonietti, M. *Angew. Chem., Int. Ed.* **2005**, *44*, 5576.
(68) Penn, R. L.; Banfield, J. F. *Am. Mineral.* **1998**, *83*, 1077.
(69) Penn, R. L.; Banfield, J. F. *Geochim. Cosmochim. Acta* **1999**, *63*, 1549.

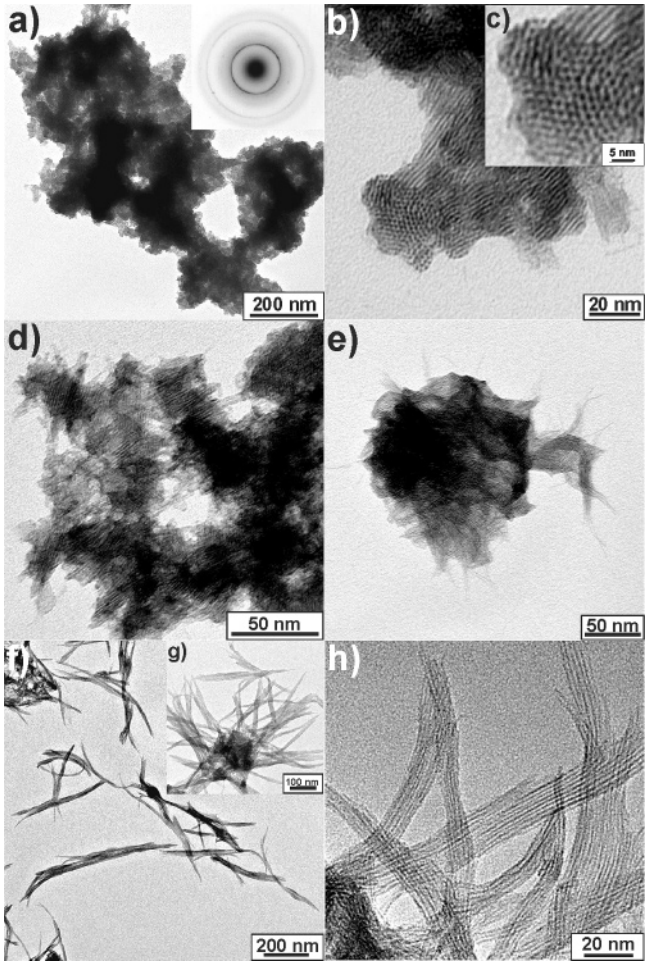

Figure 4. TEM images of tungsten oxide nanostructures synthesized at various temperatures with a constant tungsten chloride-to-DFOM molar ratio of 9. (a−c) 100 °C (inset: SAED), (d) 125 °C, (e) 150 °C, and (f−h) at 175 °C.

An overview image of the product obtained at 100 °C just shows apparently ill-defined aggregates. However, higher magnification proves the presence of a badly ordered hexagonal mesostructure, composed of wormlike organic−inorganic hybrid nanostructures (Figure 4b). Sometimes the inorganic nanowires, which appear with dark contrast, are oriented perpendicular to the copper grid, indicating the presence of a hexagonal arrangement of nanowires (Figure 4c). The highly anisotropic morphology is also reflected in the SAED pattern in Figure 4a, inset, showing two intense diffraction rings in addition to a few weaker, more diffuse ones (for more details, see below).

The nanostructures obtained at 125 °C (Figure 4d) look rather similar to the ones synthesized at 100 °C, however, with a slight increase in the length of the nanowires. This tendency is more pronounced at 150 °C, where some wires start to emerge from the larger aggregates (Figure 4e). At 175 °C, the process results in the formation of fibers only (Figure 4f), which can be curved and tangled together into starlike architectures (Figure 4g). The fiber length ranges typically from 200 to 600 nm (Figure 4f), but also longer species were found in the sample. A higher magnification TEM image gives evidence that the fibers consist of individual, single-crystalline nanowires (Figure 4h). According to Figure 4h, the flat fibers exhibit a thickness of one single nanowire, and the width typically lies between 10 and 20 nm, corresponding to 5−10 assembled nanowires. Interestingly, the

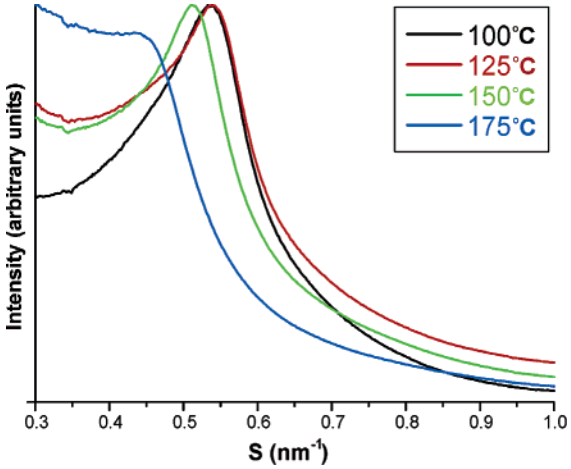

Figure 5. Small-angle X-ray scattering (SAXS) patterns of the tungsten oxide nanostructures synthesized with a constant tungsten chloride-to-DFOM molar ratio of 9 at 100, 125, 150, and 175 °C.

nanowires are mostly oriented parallel to each other, with an equal distance almost throughout the whole length of the structure.

To learn more about the long-range order of the hybrid structures and about the distances between the nanowires, small-angle X-ray scattering (SAXS) measurements were performed (Figure 5). At 100 °C, the pattern exhibits a sharp peak centered at 0.533 nm^{-1}, corresponding to an interwire distance ($d_{interwire}$) of 1.87 nm within the hexagonal structure. By increasing the temperature to 125 °C, the pattern stays practically unchanged, with a peak centered at 0.540 nm^{-1}, corresponding to a $d_{interwire}$ = 1.85 nm. At 150 °C, the peak slightly shifts toward smaller scattering vectors with a maximum around 0.513 nm^{-1} ($d_{interwire}$ = 1.95 nm). The pattern at 175 °C is less defined, with a maximum at 0.454 nm^{-1} ($d_{interwire}$ = 2.2 nm). The increase of the interwire distance with the temperature can be attributed to the increase of the diameters of the nanowires from about 0.9 nm at 100 °C to 1.3 nm at 175 °C (see HRTEM images below). The intensity distribution $I(s)$ of the SAXS patterns results from the product of the lattice factor $Z(s)$ (related to the periodicity of the nanowires) with the form factor $F(s)$ (related to the shape of the individual nanowire). In general, the width of the interference peak (∼lattice factor) is inverse proportional to the number of repeating units in a mesostructure. According to Figure 4h, the belt-like mesostructure consists only of 5−10 assembled nanowires, thus explaining the shoulder-like reflection instead of a well-resolved peak for the more extended, low-temperature structures. Independent of the temperature, the SAXS data point to the presence of an ordered arrangement of organic species between the nanowires and, additionally, give an idea about the number of nanowires assembled in the mesostructure.

The sample obtained at 175 °C was further analyzed by HRTEM, infrared spectroscopy, and elemental analysis to learn more about the crystallinity, the crystal structure, and the composition of the nanowires. The electron diffraction pattern (Figure 6a) taken from an area with several differently oriented bundles shows mainly two intense diffraction rings, similarly observed in the sample obtained at 100 °C, corresponding to the 010 and 020 reflections of the $W_{18}O_{49}$ structure (JCPDS 36-101). All other reflections are much weaker, resulting in diffuse and broad diffraction rings. This observation indicates

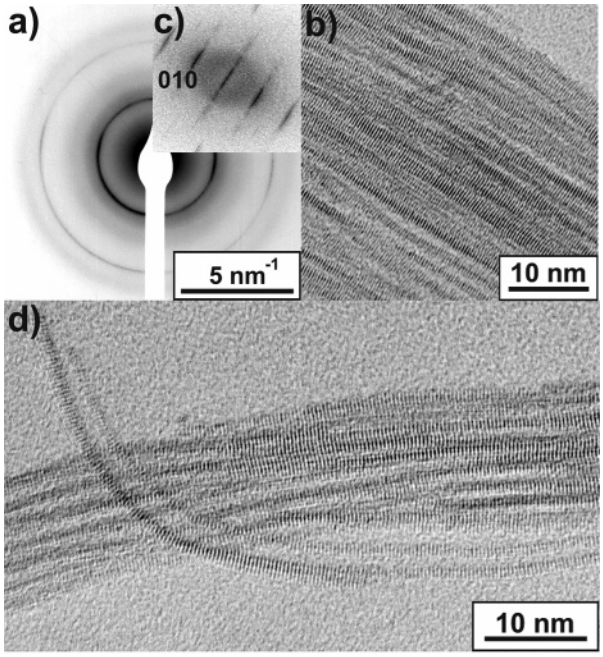

Figure 6. (a) SAED pattern of a bundle of nanowires, (b) HRTEM image of a bundle of tungsten oxide nanowires, (c) power spectrum of the HRTEM shown in (b), and (d) HRTEM image of linear and curved nanowires.

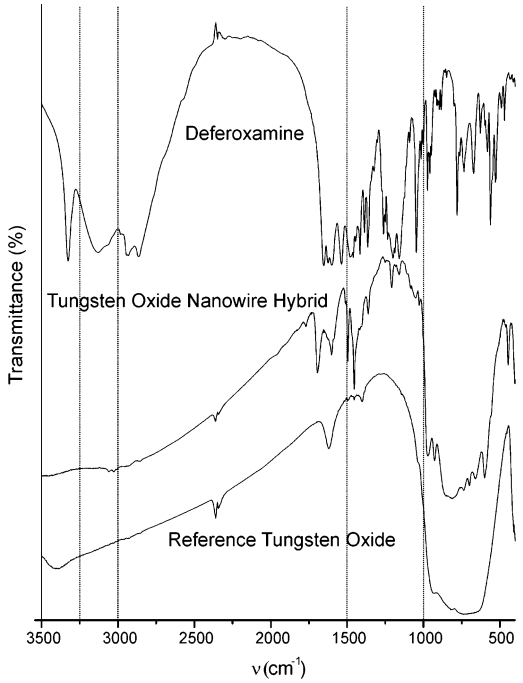

Figure 7. FT-IR spectra of the tungstite platelets obtained at 100 °C, the hybrid tungsten oxide nanowires prepared at 175 °C, and the deferoxamine mesylate salt.

that the nanowires grow along the [010] direction. It is difficult to assign the electron diffraction pattern unambiguously to a specific crystal structure because tungsten oxide forms numerous stoichiometric as well as nonstoichiometric compounds with the composition WO_{3-x} and with rather similar structures.[70] However, comparison of the experimental XRD pattern with calculations using the Debye scattering equation[23,71,72] for different tungsten oxide structures showed the best agreement for $W_{18}O_{49}$ nanowires grown along the [010] direction and with a diameter of about 1.5 nm (data not shown). The crystal structure of $W_{18}O_{49}$ is strongly anisotropic (monoclinic space group $P2/m$ $a = 1.83$, $b = 0.38$, and $c = 1.40$ nm) and consists of an ordered two-dimensional lattice of connected, edge-sharing, mutually tilted WO_6 octahedra. The $W_{18}O_{49}$ structure was reported for tungsten oxide nanowhiskers and nanorods, where the growth also occurs along the short b axis.[70,73,74] Low dose HRTEM images prove the single-crystalline nature of each nanowire (Figure 6b and d). The PS of the HRTEM image displayed in Figure 6b shows elongated spots corresponding to the 010 and 020 reflections (Figure 6c). This result is characteristic for oriented nanowires that are, however, slightly curved and misaligned with respect to each other. Figure 6d shows two strongly bent nanowires, which nevertheless keep their single-crystalline structure. The diameter of all nanowires is highly uniform, typically 1.3 nm, which is smaller than one unit cell with respect to the (010) crystal plane. This tiny lateral size is comparable to the diameter of single-walled carbon nanotubes (typically around 1.2 nm).[75] The high flexibility of the nanowires can be explained by the small cross-section, as well as by the elemental connection pattern of tungsten oxide. Obviously, bending stress can be taken up by tilting the octahedra with respect to each other.

Fourier transform infrared spectroscopy clearly shows the vibrations of an organic−inorganic hybrid structure. For comparison, FT-IR was taken from the nanowire bundles synthesized at 175 °C, deferoxamine alone, and the reference experiment without deferoxamine (Figure 7). The reference experiment shows bands at 1620 and 3400 cm^{-1}, which can be assigned to adsorbed water. In the region of 1000−500 cm^{-1}, the typical bands for W═O (950 cm^{-1}) and bridging oxygens O−W−O (600−780 cm^{-1}) appear.[76−78] The nanowire bundles prepared in the presence of deferoxamine exhibit a more complex IR spectrum. The stretching vibrations due to the tungsten oxide framework in the range of 1000−500 cm^{-1} are now split up, and an unambiguous assignment of the bands is not possible. The deferoxamine as well as the nanowire bundles feature bands in the range of 2940−2850 cm^{-1}, assignable to the stretching and bending vibrations of C−H. The three bands between 1605 and 1450 cm^{-1} are characteristic of the skeletal vibrations of an aromatic ring,[76,79] whereas the band at 1210 cm^{-1} is typical of the C−C vibration.[79] However, the lack of a band at 1018 cm^{-1}, which represents the C−O stretching of benzyl alcohol,[79] and the presence of a strong band at 1695 cm^{-1}, assignable to C═O stretching, point to the fact that benzyl alcohol is partly oxidized. This hypothesis is in agreement with the low H to C molar ratio (see below), and, as a matter of fact, the position of the C═O band corresponds well to benzaldehyde adsorbed to the surface of metal oxides.[80] This observation is further

(70) Frey, G. L.; Rothschild, A.; Sloan, J.; Rosentsveig, R.; Popovitz-Biro, R.; Tenne, R. *J. Solid State Chem.* **2001**, *162*, 300.
(71) Vogel, W. *Cryst. Res. Technol.* **1998**, *33*, 1141.
(72) Pinna, N. *Prog. Colloid Polym. Sci.* **2005**, *130*, 29.
(73) Lee, K.; Seo, W. S.; Park, J. T. *J. Am. Chem. Soc.* **2003**, *125*, 3408.
(74) Seo, J.-W.; Jun, Y.-W.; Ko, S. J.; Cheon, J. *J. Phys. Chem. B* **2005**, *109*, 5389.
(75) Iijima, S.; Ichihashi, T. *Nature* **1993**, *363*, 603.
(76) Tocchetto, A.; Glisenti, A. *Langmuir* **2000**, *16*, 6173.
(77) Chong, S. V.; Ingham, B.; Tallon, J. L. *Curr. Appl. Phys.* **2004**, *4*, 197.
(78) Ingham, B.; Chong, S. V.; Tallon, J. L. *J. Phys. Chem. B* **2005**, *109*, 4936.
(79) Caravati, M.; Grunwaldt, J.-D.; Baiker, A. *Phys. Chem. Chem. Phys.* **2005**, *7*, 278.
(80) Augugliaro, V.; Coluccia, S.; Loddo, V.; Marchese, L.; Martra, G.; Palmisano, L.; Schiavello, M. *Appl. Catal., A* **1999**, *20*, 15.

supported by the fact that bands of the carboxylate group, expected to be at around 1550 and 1410 cm^{-1},[76,81] are not present. Oxidation of benzyl alcohol to benzaldehyde using WO_3 powder as catalyst at low temperatures has been reported before.[76] It is interesting to note that in contrast to the recently reported lamellar yttrium oxide hybrid nanomaterial,[64] consisting of crystalline yttrium oxide layers with intercalated benzoate molecules, oxidation of benzyl alcohol in the tungsten oxide system does not proceed to the acid, but stops at the level of the aldehyde. Pure deferoxamine exhibits a complex IR spectrum.[82] The band near 1053 cm^{-1} can be assigned to the C−N amine stretching mode. Additional bands in the range of 2940−2850 and 1500−1280 cm^{-1} stem from stretching and bending vibrations of C−H. The peaks at 3340 and 3100 cm^{-1} correspond to N−H stretch bands of the amide overlapping with the strong O−H band of the hydroxamic groups. The amide II band, a result of the coupling of N−H bending and C−N stretching, is located at 1550 cm^{-1}. The C═O stretching absorbance appears at 1650 cm^{-1}. However, most of these bands are not present in the spectrum of the nanowire bundles, presumably due to the low content of siderophore in the hybrid structure in comparison to benzaldehyde.

Elemental analysis was performed to determine the C, H, N, and S content of the nanowire bundles obtained at 175 °C. According to these results, the ratio of these elements can be expressed by the general formula $C_{122.7}H_{135.6}N_6S_{0.15}$, which means that only a negligible amount of methanesulfonate (the counterion of the siderophore) is incorporated into the hybrid structure. The low H to C molar ratio strongly points to the presence of unsaturated organic compounds, supporting the findings of the IR investigation. Assuming that all of the nitrogen stems from DFOM, the formula can be split up into $(N_6C_{25}H_{48}O_8)(C_7H_6O)_{13.95}$, giving evidence that the nanowire bundles contain about 14 times more benzaldehyde than DFOM. Thermogravimetric analysis led to a weight loss of about 25% in the range from room temperature to 500 °C (data not shown). Taking all of the results into account (XRD, elemental analysis, and TGA), the composition of the nanowire hybrid material agrees well with the formula $WO_{2.72}(N_6C_{123}H_{136}O_{22})_{0.04}$ or $WO_{2.72}(\text{deferoxamine})_{0.04}(C_7H_6O)_{0.6}$. The final material only contains about one deferoxamine molecule per 25 tungsten atoms (which is considerably less than in the starting reaction solution).

All of these results confirm the formation of an organic−inorganic hybrid material consisting of tungsten oxide nanowires with a sheath of benzaldehyde and presumably a few deferoxamine molecules. Although there is no direct information about the nature of the attractive forces, it is reasonable to assume that van der Waals interactions plus some directional amide bonds provided by the deferoxamine molecules hold the nanowires together. Consequently, it should be possible to separate the nanowire bundles into individual species by chemical means. To achieve that, a few drops of the hybrid bundles dispersed in ethanol were added to various solvents, such as water, formamide, chloroform, and diethyl ether. Individual nanowires were observed in formamide only. Obviously, only a protic solvent with a particularly high polarity is able to break the interactions between the nanowires. It is interesting to note that, although no nanowire bundles are present anymore, only few nanowires were found on the TEM grid (Figure 8). This observation points to the possibility that formamide is able to destroy them partially.

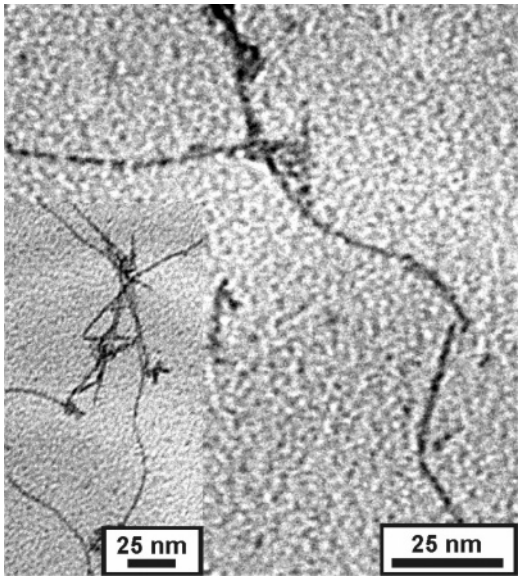

Figure 8. TEM images of individual tungsten oxide nanowires after treatment with formamide at different magnifications.

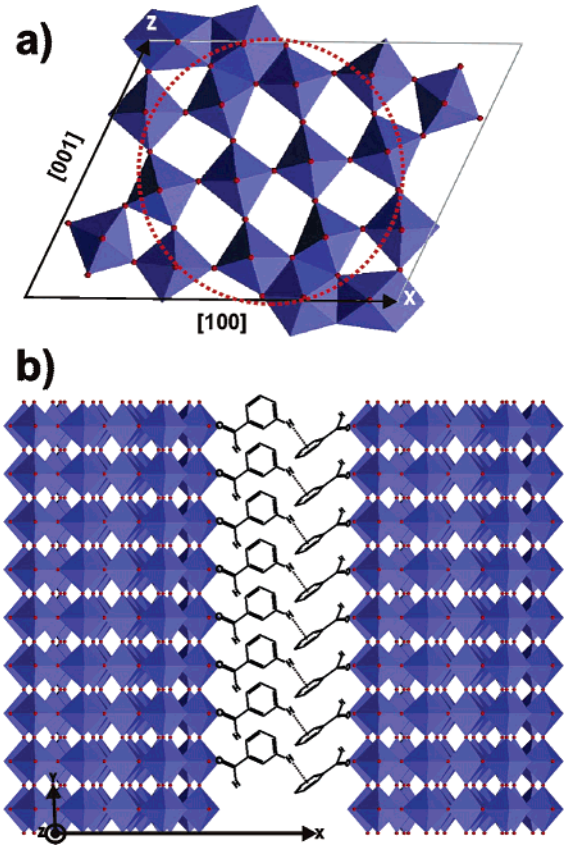

Figure 9. Schemes representing (a) the cross section of a 1.3 nm nanowire inside one $W_{18}O_{49}$ unit cell oriented along the [010] direction and (b) the proposed model for the nanohybrid structure.

All of the data presented before can be summarized in a structure model for the nanowire assembly (Figure 9). A comparison of the unit cell of $W_{18}O_{49}$ projected along the [010] direction with the typical diameter of the nanowires of 1.3 nm

(81) Koutstaal, C. A.; Ponec, V. *Appl. Surf. Sci.* **1993**, *70/71*, 206.
(82) Yehuda, Z.; Hadar, Y.; Chen, Y. *J. Agric. Food Chem.* **2003**, *51*, 5996.

(red circle) allows a rough estimation of the proportion of tungsten atoms present on the nanowire surface (Figure 9a). The cross section in the (101) plane contains 12−14 tungsten atoms, and about 7 of them are located on the surface. The parallel alignment of the nanowires with respect to each other in the as-synthesized product indicates the presence of an ordered, supramolecular arrangement of the intercalated organic molecules. The thickness of the organic layer, that is, the distance between the surfaces of two nanowires, is about 0.9 nm (difference between the interwire distance of 2.2 nm and the diameter of a single nanowire of 1.3 nm).

We believe that the hybrid structure is formed via a cooperative growth and assembly process. After the addition of deferoxamine to the tungsten chloride solution in benzyl alcohol, various mono- as well as polynuclear tungsten−deferoxamine complexes form, easily monitored by several color changes of the reaction solution. Deferoxamine contains three hydroxamic acid groups, which are involved in coordination. The amide group generally remains uncoordinated. In biological systems, the three hydroxamic acid groups are distributed in a way that they are able to coordinate to the same metal ion. However, in the present case the molar excess of tungsten relative to deferoxamine should favor the formation of multinuclear binding. Upon heating, these species induce the anisotropic growth of the nanowires. Previously published work by other research groups provides some information about the possible orientation of the phenyl rings with respect to each other. Generally, in benzene derivatives the most stable dimer does not correspond to the parallel sandwich structure, but to the T-shaped structure via attractive "edge-to-face" interactions (Figure 9b).[83] The adsorption of benzaldehyde onto the (001) crystal face of TiO_2 occurred in a way that the phenyl rings exhibited a tilt angle of 54° with respect to the oxide surface.[84] The coordination of a large number of benzaldehyde molecules to the Lewis acid sites on the tungsten oxide nanowire surface leads to an additional lowering of the surface energy and a stabilization of the overall structure.

Conclusions

The synthesis of metal oxide nanostructures in the presence of low molecular weight biomolecules in organic solvents is unusual, but particularly fascinating, because it allows an elegant combination of bioinspired morphosynthesis with nonaqueous sol−gel chemistry. In this combination, a small amount of biomolecules controls the crystal growth and presumably also the assembly behavior of the inorganic compounds, enabling the synthesis of crystalline nanomaterials with complex morphology at rather low reaction temperatures.

Because bulk tungsten oxide exhibits manifold application potential, including electrochromism, semiconductivity, catalytic activity, and sensing properties, it can be expected that nanowires with diameters of about 1 nm possess novel and interesting properties. Especially the highly flexible construction principle of tungsten oxides gives rise to the reasonable expectation that the conductivity of the nanowires will depend on the degree of deformation, while overall conductance level will depend on the oxidation state.[85] Accordingly, the directed assembly of such nanowires makes them ideal candidates for multi-purpose sensing materials. In addition, the organic coating enables separation, dispersion, and a rational interfacing of those nanostructures, either to other functional organic units or for assembling onto patterned arrays via the deferoxamine or benzaldehyde moieties.

Acknowledgment. Financial support from the Max-Planck-Society and from the DFG (Priority program SPP 1165 "Nanodrähte und Nanoröhren") is gratefully acknowledged. We thank the Fritz-Haber-Institute and Prof. R. Schlögl for the use of the electron microscope and Klaus Weiss for his technical assistance.

JA0544915

(83) Muller-Dethlefs, K.; Hobza, P. *Chem. Rev.* **2000**, *100*, 143.
(84) Sherrill, A. B.; Lusvardi, V. S.; Eng, J., Jr.; Chen, J. G.; Barteau, M. A. *Catal. Today* **2000**, *63*, 43.
(85) Aird, A.; Domeneghetti, M. C.; Mazzi, F.; Tazzoli, V.; Salje, E. K. H. *J. Phys.: Condens. Matter* **1998**, *10*, L569.